IMPLEMENTATION OF ACTIVE-ANTI ROLL BAR CONTROL SYSTEM TO A 3-AXLE DOUBLE-DECKER BUS

Vijayapragas Muniandy[1*], Tze Peng Loo[2], Jeyagopi Raman[3], Sudesh Nair Baskara[4]

Abstract

Double-decker buses have the potential to save space in the traffic, but their center of gravity is high, which will cause a higher roll angle and discomfort to the passengers. In this paper, the existing control system of active anti-roll bars was tuned, implemented and modified specifically for double-decker buses. A full car ride and handling, 3-axle simulation model consisting of 20 degrees of freedom (DOF) was modeled and simulated within Matlab/ Simulink environment. The controller proposed in this research is self-tuning fuzzy logic PID controller. A series of scenarios were tested, which are half bump, U-turn, double lane change (ISO3888-1) and moose test (ISO3888-2). For all the tests, main priority of performance improvement will be to focus on roll angle, roll rate, bounce motion and lateral acceleration. On average, active anti-roll bar (ARB) can improve the performance up to at least 90% compared to passive ARB, however lateral acceleration will be scarified by about 2.22% on average. Such small degradation on lateral accelerations performances on a double-decker bus will not affect safety negatively due to slower speed of the vehicle.

Received: *11 June, 2025*
Revised: *26 November, 2025*
Accepted: *29 December, 2025*

[1,3,4]Department of Mechanical Engineering, Faculty of Engineering and Quantity Surveying, Inti International University, Persiaran Perdana BBN, Putra Nilai, 71800, Nilai, Negeri Sembilan, Malaysia.

[2]Department of Mechanical Engineering, Faculty of Engineering and Technology, Tunku Abdul Rahman University of Management and Technology, Jalan Genting Kelang, Setapak, 53300, Kuala Lumpur, Malaysia.

****Corresponding author:***
vijay.muniandy@newinti.edu.my

DOI: *https://doi.org/10.54552/v87i1.302*

Keywords:
Active anti-roll bar, Bus dynamics, 3-axle, Fuzzy PID

1.0 INTRODUCTION

In developing countries like Malaysia, the population rate and the number of car owners have increased dramatically, which causes traffic problems to increase exponentially as well (Solah *et. al.,* 2013). A high-deck double-decker bus has slowly been implemented by public transport company, which is a good solution for this situation. However, high deck double-decker buses are known to be dangerous as they are easy to cause accidents, more specifically rollover accidents (Solah *et. al.,* 2013).

Rollover accidents are fatal to passengers and traffic around them, the cause of rollover accidents is due to lateral stability loss. Sided wind gusts, abrupt steering and braking maneuver by the driver are the three major factors for rollover accidents (Solah *et. al.,* 2013; Gauchia *et. al.,* 2010; Gillespie, 2021; Kuo & Li, 1999; Vu *et. al.,* 2016; Vu, 2017). All these factors will cause one side of the vehicle wheel to leave off the ground and cause the normal force of tire and road to be zero when it reaches the threshold of roll angle, rollover accident starts. In this study, only abrupt steering input and its effects will be considered.

There are a few proposed methods to overcome body roll such as active steering control, which will affect the yaw motion to modify the rate of steering angle with a given different speed input. Other than that, active brake system will give a small brake force to each of the wheels (Gillespie, 2021; Vu *et. al.,* 2016). Although this is a good method to keep every wheel with the least slip angle to prevent understeer or oversteer and it also has the ability to detect a dangerous situation, the brake system will reduce the lateral tire force, which is responsible for the rollover (Gillespie, 2021; Vu *et. al.,* 2016; Manap *et. al.,* 2016). Next, active anti-roll bar is another advanced method to control excessive body roll, which usually pairs with hydraulic actuators, electric motor or pneumatic actuators to add or dissipate energy to the vehicle suspension system (Gauchia *et. al.,* 2010; Gillespie, 2021; Vu, 2017; Muniandy *et. al.,* 2015). When the center of gravity of the sprung mass is leaving the centerline, the sensors will detect the moment then by using the force of hydraulic actuators to react at the moment of vehicle body roll (Brian, 2002; Conover, 2004); this reaction will give the vehicle sufficient roll stiffness to stay flat relative to the road.

From the literature review, it can be concluded that active anti-roll bar (A.ARB) is suitable to be used to solve the problem of rollover accidents. The reason to eliminate the other two methods is that active steering control will also modify the desired path of the vehicle, affecting the yaw motion, and the active brake system will only activate when the wheel reaches nearly the limit of lift-off (Vu *et. al.,* 2016; Noraishikin *et. al.,* 2014). Both disadvantages mentioned could cause heavy vehicles to easily lose control and endanger the people around it. In this research, it is suggested to choose hydraulic linear actuators for the proposed A.ARB system due to the higher

force generation capability, suitable for heavy vehicles like double-decker bus (Brian, 2002; Conover, 2004; Noraishikin *et. al.,* 2014).

To understand rollover events, according to (Vu, 2017), the rollover of heavy vehicles can be classified into four types, which are preventable, potentially preventable, non-preventable and preventable unknown. Although there are different types of rollover events with different levels of dangerous levels, the study shows that minority of rollover accidents could have been avoided with a warning device, but the majority were not preventable by driver action alone (Vu *et. al.,* 2016; Vu, 2017). Because the rollover angle threshold is too small for the driver to feel the "vehicle is rolling", so the vehicle has already undergone rollover before the driver realises it (Vu *et. al.,* 2016; Vu, 2017). According to Gillespie (2021), the rollover threshold is 5.886 m/s as for the base model that will be used in this paper, Enviro 500 double-decker bus. Since before this paper there are no specific 3-axle double-decker vehicle models presented in any literature, the author of this paper developed a new Full car 20 DOF mathematical model to simulate the 3-axle double-decker bus ride and handling motion. The details of the model will be explained in the next section.

2.0 RIDE AND HANDLING FULL 3-AXLE VEHICLE MATHEMATICAL MODEL

In this paper the author will modify and derive from existing 2-axle vehicle from (Gillespie, 2021; Muniandy *et. al.,* 2015; Abu et. al., 2014; Darus & Yahaya, 2009; Frey, 2009; Ahmed, 2017; Joga *et. al.,* 2009) to a new 3-axle vehicle mathematical model. In riding, comfort models consist of vehicle body roll, pitch and bounce motion with 6 vertical motions from the wheels resulting in 9 DOF. In handling model, it consists of vehicle body roll, pitch, lateral and longitudinal motion with 6 rotational motions from the wheels, resulting in 11 DOF. Full car, 3-axle mathematical model is the combination of the 2, therefore results in 20 DOF.

2.1 Ride Comfort Model for 3-Axle Full Vehicle (9DOF)

Figure 1 shows full car ride and handling model for 3-axle vehicle. Indication i and j will be used in this paper. Whereas i = 1, 2 and 3 for position of axle and j = 1 for left and 2 for right. The following equations will be derived based on Figure 1.

Vertical displacement and velocity equations for 3-axle vehicle

$$Z_{s11} = -\frac{w}{2}\varphi_b + l_1\theta_b + Z_b \quad (1)$$

$$\dot{Z}_{s11} = -\frac{w}{2}\dot{\varphi}_b + l_1\dot{\theta}_b + \dot{Z}_b \quad (2)$$

Where Z_{sij} is the vertical displacement of sprung mass on the location point of wheel, Z_b is the vertical displacement of body mass (center of gravity). α_b is the pitch angle of the vehicle, θ_b is the roll angle of the vehicle and L_i is the length of the axle to the centre of gravity. In equation 1 and 2, the term $\frac{w}{2}\varphi_b$ and $\frac{w}{2}\dot{\varphi}_b$ is negative at j = 1 and positive at j = 2, the term $l_i\theta_b$ and $l_i\dot{\theta}_b$ s positive at i = 1 and negative at i = 2,3.

Bounce motion for 3-axle vehicle

$$\ddot{Z}_b = \frac{1}{M}(C_{11}(\dot{Z}_{u11} - \dot{Z}_{s11}) + K_{s11}(Z_{u11} - Z_{s11}) + C_{12}(\dot{Z}_{u12} - \dot{Z}_{s12}) + K_{s12}(Z_{u12} - Z_{s12}) + C_{21}(\dot{Z}_{u21} - \dot{Z}_{s21}) + K_{s21}(Z_{u21} - Z_{s21}) + C_{22}(\dot{Z}_{u22} - \dot{Z}_{s22}) + K_{s22}(Z_{u22} - Z_{s22}) + C_{31}(\dot{Z}_{u31} - \dot{Z}_{s31}) + K_{s31}(Z_{u31} - Z_{s31}) + C_{32}(\dot{Z}_{u32} - \dot{Z}_{s32}) + K_{s32}(Z_{u32} - Z_{s32})) \quad (3)$$

Roll motion for 3-axle vehicle

$$\ddot{\varphi}_b = \frac{1}{I_{xx}}(-C_{11}w_{11}(\dot{Z}_{u11} - \dot{Z}_{s11}) - K_{s11}w_{11}(Z_{u11} - Z_{s11}) + C_{12}w_{12}(\dot{Z}_{u12} - \dot{Z}_{s12}) + K_{s12}w_{12}(Z_{u12} - Z_{s12}) + T_{ar1} - C_{21}w_{21}(\dot{Z}_{u21} - \dot{Z}_{s21}) - K_{s21}w_{21}(Z_{u21} - Z_{s21}) + C_{22}w_{22}(\dot{Z}_{u22} - \dot{Z}_{s22}) + K_{s22}w_{22}(Z_{u22} - Z_{s22}) + T_{ar2} - C_{31}w_{31}(\dot{Z}_{u31} - \dot{Z}_{s31}) - K_{s31}w_{31}(Z_{u31} - Z_{s31}) + C_{32}w_{32}(\dot{Z}_{u32} - \dot{Z}_{s32}) + K_{s32}w_{32}(Z_{u32} - Z_{s32}) + T_{ar3}) \quad (4)$$

Pitch motion for 3-axle vehicle

$$\ddot{\theta}_b = \frac{1}{I_{yy}}(-C_{11}l_1(\dot{Z}_{u11} - \dot{Z}_{s11}) - K_{s11}l_1(Z_{u11} - Z_{s11}) - C_{12}l_1(\dot{Z}_{u12} - \dot{Z}_{s12}) - K_{s12}l_1(Z_{u12} - Z_{s12}) + C_{21}l_2(\dot{Z}_{u21} - \dot{Z}_{s21}) + K_{s21}l_2(Z_{u21} - Z_{s21}) + C_{22}l_2(\dot{Z}_{u22} - \dot{Z}_{s22}) + K_{s22}l_2(Z_{u22} - Z_{s22}) + C_{31}l_3(\dot{Z}_{u31} - \dot{Z}_{s31}) + K_{s31}l_3(Z_{u31} - Z_{s31}) + C_{32}l_3(\dot{Z}_{u32} - \dot{Z}_{s32}) + K_{s32}l_3(Z_{u32} - Z_{s32})) \quad (5)$$

K_{sij} is the spring stiffness of the spring in sprung mass on each wheel, C_{ij} is the damping coefficient of the absorber in suspension on each wheel. Z_{uij} and Z_{sij} is the vertical displacement of unsprung and sprung mass, $\dot{Z}_{uij}$ and $\dot{Z}_{sij}$ is the vertical velocity of unsprung and sprung mass. M is the total mass of the vehicle I_{xx} is the moment of inertia about x-axis (roll axis), I_{yy} is the moment of inertia about y-axis (pitch axis) and $\ddot{Z}_b$ is vehicle body bounce acceleration, $\ddot{\varphi}_b$ is the vehicle body roll acceleration and $\ddot{\theta}_{bis}$ the vehicle body pitch acceleration. Figure 2 shows the free body diagram for an anti-roll bar.

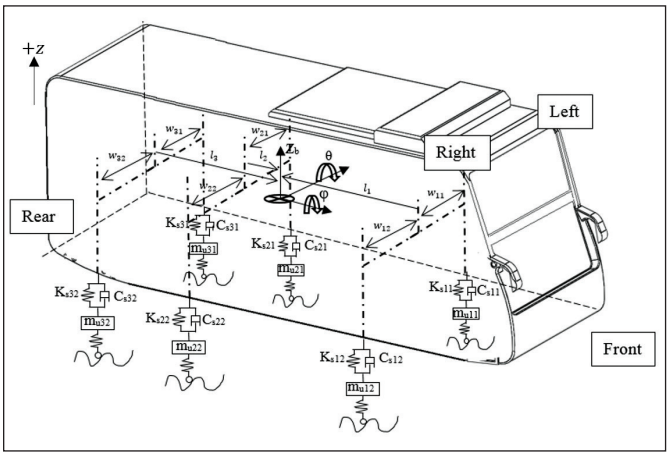

Figure 1: Ride comfort free body diagram for 3-axle vehicle

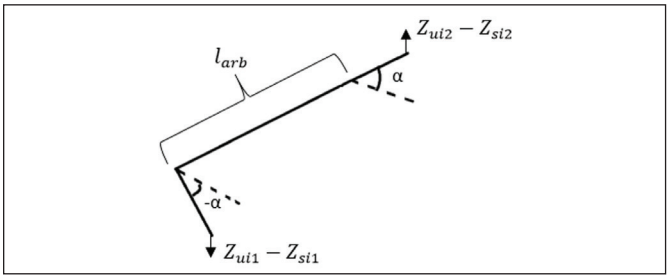

Figure 2: Free body diagram of anti-roll bar

Acceleration of unsprung mass for 3-axle vehicle

$$m_{uij}\ddot{Z}_{uij} = C_{ij}(\dot{Z}_{uij} - \dot{Z}_{sij}) + K_{sij}(Z_{uij} - Z_{sij}) - K_{tij}(Z_{rij} + Z_{uij}) - (\frac{K_{ri}}{w_{ij}})\alpha \quad (6)$$

m_{uij} is the unsprung mass, $\ddot{Z}_{uij}$ is the vertical acceleration of unsprung mass, K_{tij} is the tyre stiffness and K_{ri} is the passive anti-roll bar stiffness (P.ARB). The term $(\frac{K_{ri}}{w_{ij}})\alpha$ negative at j = 1 and positive at j = 2.

2.2 Handling Model for 3-Axle Full Vehicle (11DOF)

By referring to Figure 3, yaw motion with aligning moment for 3-axle vehicle can be derived as follows:

$$I_{zz}\dot{\psi}_z = l_1(F_{x11}+F_{x12})\sin\delta + l_1(F_{y11}+F_{y12})\cos\delta - l_2(F_{y21}+F_{y22}) + \frac{w_1}{2}(F_{x12}-F_{x11})\cos\delta + \frac{w_2}{2}(F_{x22}-F_{x21}) + \frac{w_1}{2}(F_{y11}-F_{y12})\sin\delta - l_3(F_{y31}+F_{y32}) + \frac{w_3}{2}(F_{x32}-F_{x31}) + M_{z11}+M_{z12}+M_{z21}+M_{z22}+M_{z31}+M_{z32} \quad (7)$$

Where I_{zz} is the moment of inertia about z-axis, $\dot{\psi}_z$ is the angular velocity of yaw of the vehicle, l_i is the length from axle i to the centre of gravity, w_i is the width of the vehicle track and M_{zij} is the alignment moment.

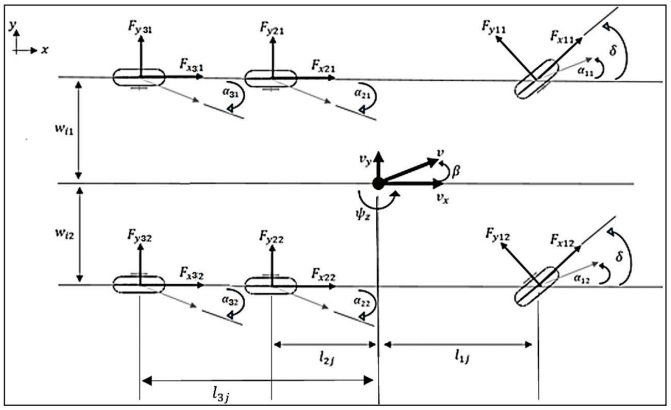

Figure 3: Free body diagram of planar of 3-axle vehicle

Longitudinal motion for 3-axle vehicle

$$a_x - v_y\psi_z = \frac{1}{M}[(F_{x11}+F_{x12})\cos\delta - (F_{y11}+F_{y12})\sin\delta + F_{x21}+F_{x22}+F_{x31}+F_{x32}] \quad (8)$$

Where a_x is the acceleration of the vehicle in x-direction and v_y is the velocity of the vehicle in y-direction. ψ_z is the yaw angle of the vehicle and δ is the steering angle on the front wheels. F_{xij} and F_{yij} are forces on wheel in x and y direction. F_x is the longitudinal force on the wheel and F_y is the lateral forces on the wheel and δ is steering angle.

Lateral motion for 3-axle vehicle

$$a_y + v_x\psi_z = \frac{1}{M}[(F_{y11}+F_{y12})\cos\delta - (F_{y11}+F_{y12})\sin\delta + F_{y21}+F_{y22}+F_{x31}+F_{x32}] \quad (9)$$

Where ψ_z is the yaw angle, a_y is the acceleration of the vehicle in y-direction and v_x is the velocity of the vehicle in x-direction.

Brake model for 3-axle vehicle

$$I_\omega\dot{\omega}_{ij} = T_{aij} - T_{bij} - F_{xij}R_w \quad (10)$$

Where I_ω is the moment of inertia of the wheel about ω-axis. T_a and T_b are torque due to acceleration and torque due to braking. The F_f is the frictional force created between road and tyre. Lastly R_w is the radius of the wheel.

Lateral slip angle for 3-axle vehicle

$$\alpha_{ij} = \tan^{-1}\left(\frac{v_y + l_i\psi_z}{v_x}\right) - \delta \quad (10.1)$$

In equation (10.1), the steering angle, δ is only apply on i = 1 axle and the term $l_i\,\psi_z$ is negative at i = 2, 3 positive at i = 1.

Longitudinal slip ratio model for 3-axle vehicle

$$V_{tii} = \sqrt{(v_y + l_i\dot{\Psi})^2 + (v_x + w_i\psi)^2} \quad (11)$$

$$v_{Lxi} = V_{ti1}\cos\alpha_{1j} \quad (12)$$

$$S_{\alpha ij} = \frac{v_{Lxi} - \omega_i R_w}{v_{Lxi}} \quad (13)$$

Note that, the term $l_2\dot{\Psi}$ in equation (11) will be negative at i = 2, 3

Load transfer for 3-axle vehicle

$$F_{zijLT} = m_{0ij}g - m_s\frac{d_p}{l_1}a_x - m_s\frac{d_{rc}}{w}a_y - F_{zij} \quad (14)$$

F_{zijLT} is the load transfer on vehicle body wheel sides, m_{011} is the initial weight experience by the vehicle, d_{rc} is the distance from CG to roll axis, d_p is the distance from CG to pitch axis and F_{zij} is the vertical force on vehicle body wheel sides. In equation (14), the term $m_s\frac{d_p}{l_1}a_x$ is negative at i = 1 positive at i = 2, 3 and the term $m_s\frac{d_{rc}}{w}a_y$ is negative at j = 1 and positive at j = 2. Note that vehicle roll and pitch motion due to handling is similar with 2-axle vehicle (Muniandy *et. al.,* 2015; Darus & Yahaya, 2009; Uil *et. al.,* 2007).

2.3 Magic Formula

The latest Pacejka tyre model is PAC2002 (Adams, 2024; Hans, 2012) and is used in this paper. However, simplification is possible due to some insignificant factors included in the model. For example, like tyre pressure, effective rolling radius, rolling resistance moment and overturning moment. Moreover, Enviro 500 camber angle is 0.

3.0 PARAMETERS

Basic parameters of Enviro 500 Double-decker Bus can be found in the catalogue as shown in Table 1 (Abu, 2014; Prochowski & Zielonka, 2014; Slade, 2009; Belrzaeg *et. al.,* 2021).

As for PAC2002 parameters for 315/80 R22.5 tyres are obtainable from Adams tyre library files. Overall simulation model built in MATLAB Simulink software is shown in Figure 4.

Table 1: Enviro 500 parameters

Parameter	Value	Parameter	Value	Parameter	Value
l_{1CG}	4.7151 m	m_{031}, m_{032}	5000 kg	K_r	99195.9348 $\frac{Nm}{rad}$
l_{2CG}	1.2779 m	m_{u1}	406.8 kg	C_r	80900 $\frac{Nm}{s\cdot rad}$
l_{3CG}	2.5779 m	m_{u2}	513.6 kg	k_{ARB1}	100730 $\frac{Nm}{rad}$
h_{ra}	0.648 m	I_{xx}	49000 m^4	k_{ARB2}	105400 $\frac{Nm}{rad}$
h_{cgx}	5.25 m	I_{yy}	411000 m^4	k_{ARB3}	108500 $\frac{Nm}{rad}$
h_{cgy}	0 m	I_{zz}	396000 m^4	k_{s21}, k_{s22}, k_{s31}, k_{s32}	452000 Nm
h_{cgz}	1.43 m	I_w	15.1070 m^4	C_{11}, C_{12}	38789.9 $\frac{Nm}{s}$
M	24000 kg	l_{a1}	0.4318 m	C_{21}, C_{22}	53026.4 $\frac{Nm}{s}$
M_s	21345.6 kg	l_{a2}	0.4826 m	C_{31}, C_{32}	10480.3 $\frac{Nm}{s}$
w	2.545 m	l_{a3}	0.5588 m	K_p	881700 $\frac{Nm}{rad}$
m_{011}, m_{012}, m_{021}, m_{022}	3750 kg	k_{s11}, k_{s12}	387000 Nm	C_p	888203.5 $\frac{Nm}{s\cdot rad}$

3.1 Inputs

The half bump test input is by giving dimension from Figure 5 to the model with different travel and delay time according to the speed.

In handling test, steering dynamics formula was constructed as the input graphs for the tests. Equations $\delta_0 = \frac{l}{R+\frac{w}{2}}$, $\delta_i = \frac{l}{R-\frac{w}{2}}$ and $\cot\delta = \frac{\cot\delta_0 + \cot\delta_0}{2}$ will be used (Harnoor *et. al.,* 2025). All the road specification is following the standard set in (Jabatan Kerja Raya, 1985; ISO 3888-1, ISO 3888-2) the

example results of 40 km/h tests input is shown below. Figures 6 and 7 show the input signals used for the simulation purpose in this research.

The input signals shown in Figures 6 and 7 are based on proper industrial standards.

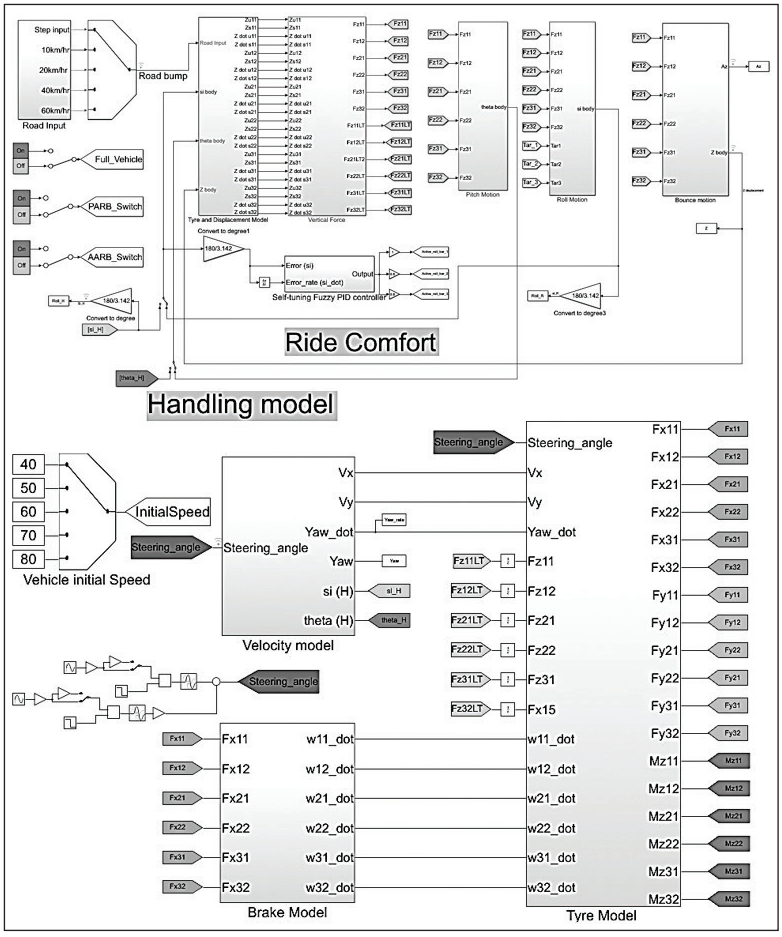

Figure 4: Overview of Full car, 3-axle vehicle mathematical model in Simulink

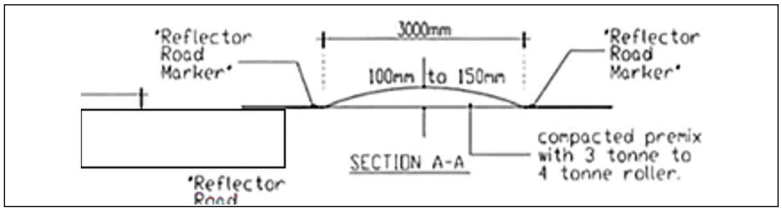

Figure 5: Specification of road bump (Jabatan Kerja Raya, 2015)

3.2 Controller

The chosen controller is self-tuning fuzzy PID controller, which has been tested in active suspension system before by various researchers. It is found that this controller is robust and suitable for high vibration applications. The self-tuning fuzzy PID controller structure is shown in Figure 8.

The diagram shown in Figure 8 is the actual Simulink model for the PID controller, with reference signal of constant zero fed into the controller. In this paper, it is found that k_p = 300000, k_i = 17500 and k_d = 8500 is best compared to other values. These values merely act like amplifiers to suit the required total force of A.ARB system. The active forces will then be distributed to each axle at 1:0.8:0.8 ratio. The Fuzzy logic memberships and rules studied from (Muniandy *et. al.,* 2015; Pivonka, 2002; Ross, 2010).

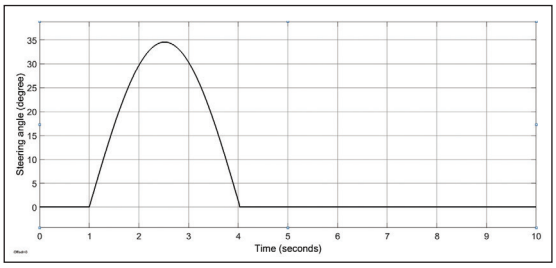

Figure 6: Steering input for U-turn test at 40km/h

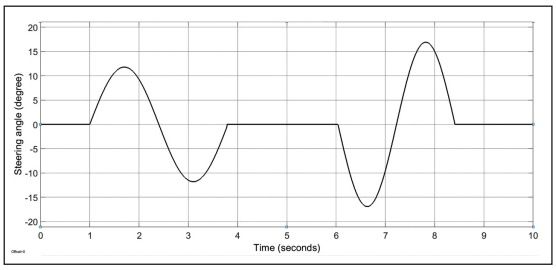

Figure 7: Steering input for ISO3888-1 test at 40km/h

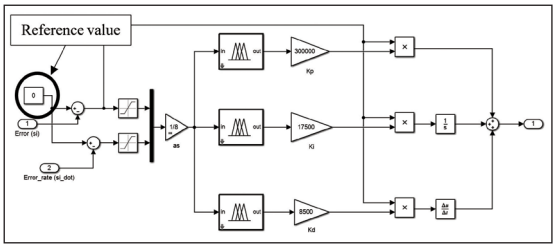

Figure 8: Roll angle result from half bump test at 40km/h

4.0 RESULTS AND DISCUSSION

4.1 Half Bump Test at 60km/h

Figures 9 to 12 show the results comparison for both passive and active anti-roll bar system for 40 km/h half bump test.

It can be seen from Figures 9 – 12, A.ARB system do have less excitation magnitude and quicker settling time compared to P.ARB. For example, in Figure 9, it can be seen the roll angle maintain within the margin of error of 0 degree, leaving the vehicle stay flat even after hitting the bump at 40km/h. Ride comfort has also been approved as evidence shown in Figure 12, as vertical acceleration is reduced by 22.05%. Further tests have been carried out to ensure the proposed controllers' robustness and repeatability.

4.2 U-turn (180-degree turn) test at 80km/h

Figures 13 to 15 show the results comparison for both passive and active anti-roll bar system for 80 km/h U-Turn test.

For handling tests, steering angle was used as input rather than road profile input as shown in previous half bump test. Again, similar to the half bump tests, Figures 13 – 15 also show that A.ARB system does have less excitation magnitude and quicker settling time compared to P.ARB.

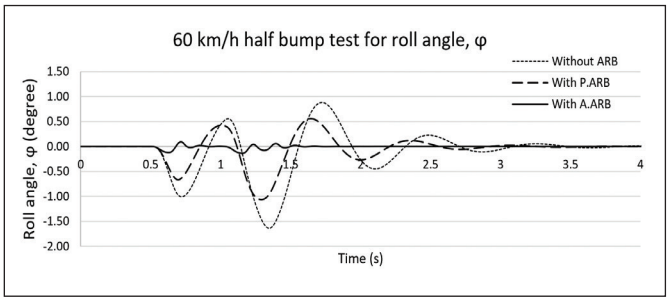

Figure 9: Roll angle result from half bump test at 40km/h

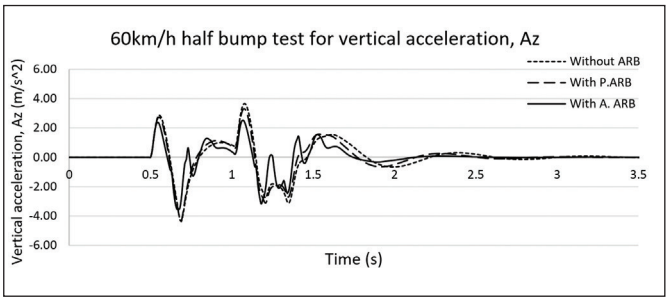

Figure 12: Vertical acceleration results from half bump test at 40km/h

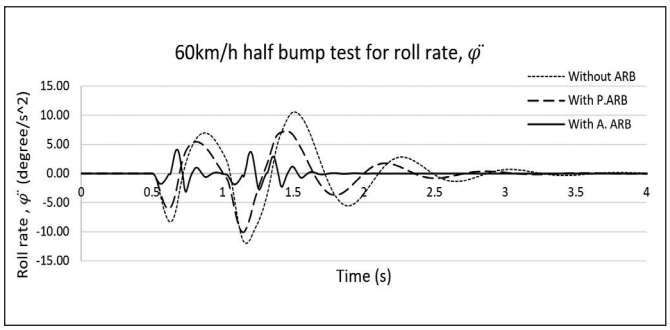

Figure 10: Roll rate result from half bump test at 40km/h

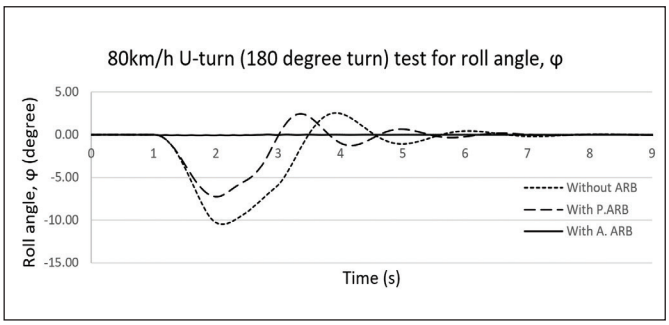

Figure 13: Roll angle result from 80km/h U-turn test

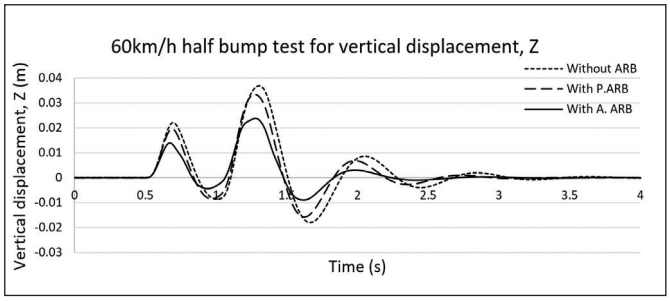

Figure 11: Vertical displacement result from half bump test at 40km/h

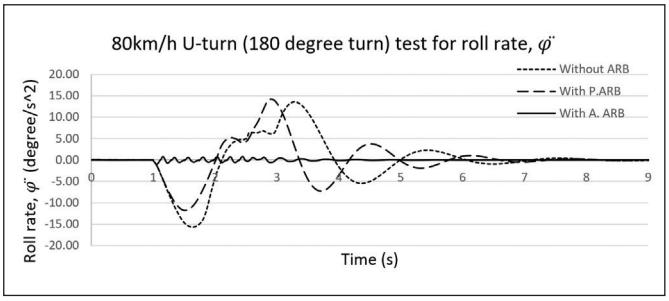

Figure 14: Roll rate result from 80km/h U-turn test

Table 2: RMS value comparison from half bump test at 40km/h

				Improvement of performance RMS comparison (%) between		
				Without ARB and		With P.ARB and
	Without ARB	**With P.ARB**	**With A.ARB**	**With P.ARB**	**With A.ARB**	**With A.ARB**
Roll angle	0.3617	0.2290	0.0219	36.68	93.93	90.42
Roll rate	3.0139	2.1169	0.6073	29.76	79.85	71.31
Z	0.0078	0.0068	0.0047	12.33	39.33	30.79
Az	0.7834	0.7558	0.5892	3.51	24.79	22.05

Table 3: RMS value comparison from U-turn test at 80km/h

				Improvement of performance RMS comparison (%) between		
				Without ARB and		With P.ARB and
	Without ARB	**With P.ARB**	**With A.ARB**	**With P.ARB**	**With A.ARB**	**With A.ARB**
Roll angle	4.1400	2.6505	0.0310	35.98	99.25	98.83
Roll rate	6.1502	5.1629	0.2337	16.05	96.20	95.47
Ay	1.7170	1.7700	1.5371	1.77	10.47	13.16

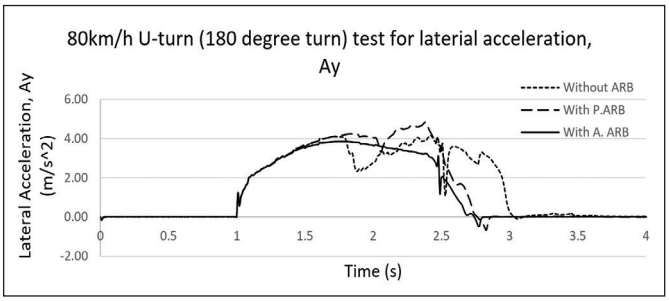

Figure 15: Lateral acceleration results from 80km/h U-turn test

4.3 Double lane change test (ISO 3888-1) at 80km/h

Figures 16 to 18 show the results comparison for both passive and active anti-roll bar system for 80 km/h double lane change test.

Figures 16 – 18 also shows similar trend in the differences of passive and active anti-roll bar performances.

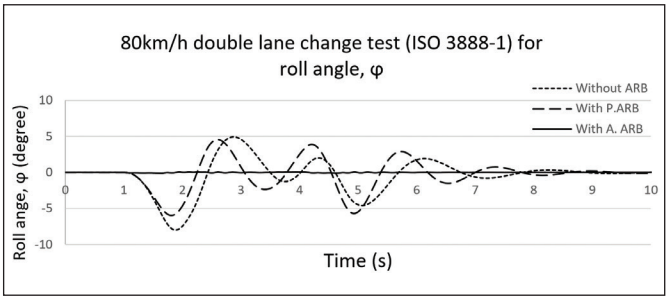

Figure 16: Roll angle result from 80km/h ISO 3888-1 test

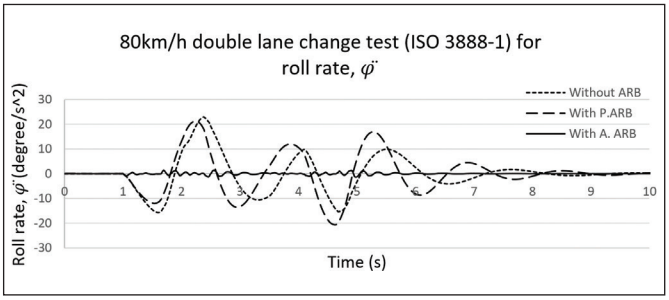

Figure 17: Roll rate result from 80km/h ISO 3888-1 test

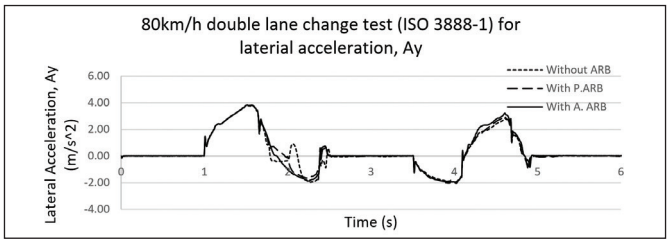

Figure 18: Lateral acceleration results from 80km/h ISO 3888-1 test

4.4 Handling moose test (ISO 3888-2) at 80km/h

Figures 19 to 21 show the results comparison for both passive and active anti-roll bar system for 80 km/h handling moose test.

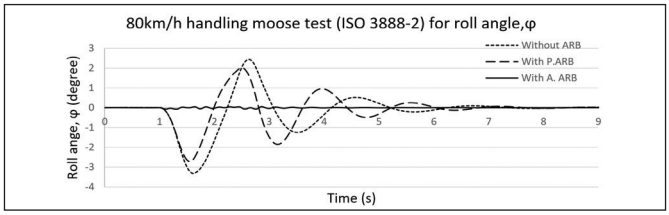

Figure 19: Roll angle result from 80km/h ISO 3888-2 test

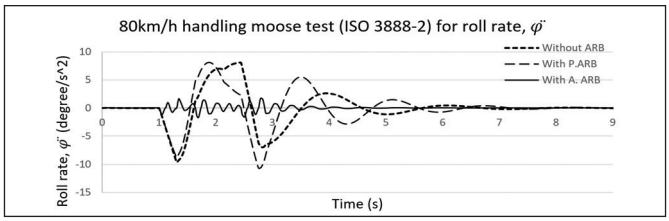

Figure 20: Roll rate result from 80km/h ISO 3888-2 test

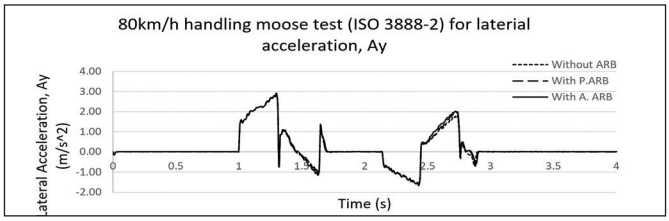

Figure 21: Lateral acceleration results from 80km/h ISO 3888-2 test

Table 4: RMS value comparison from ISO 3888-1 test at 80km/h

				Improvement of performance RMS comparison (%) between		
				Without ARB and		With P.ARB and
	Without ARB	With P.ARB	With A.ARB	With P.ARB	With A.ARB	With A.ARB
Roll angle	2.9618	2.6546	0.0319	10.37	98.92	98.80
Roll rate	8.6206	9.7639	0.4362	-13.26	94.94	95.53
Ay	1.2425	1.2608	1.3133	1.26	-5.69	-4.16

Table 5: RMS value comparison from ISO 3888-2 test at 80km/h

				Improvement of performance RMS comparison (%) between		
				Without ARB and		With P.ARB and
	Without ARB	With P.ARB	With A.ARB	With P.ARB	With A.ARB	With A.ARB
Roll angle	1.1068	0.9440	0.0208	14.72	98.12	97.80
Roll rate	3.4744	3.6139	0.4371	-4.02	87.42	87.90
Ay	0.6048	0.6135	0.6214	0.61	-2.74	-1.28

Lower vehicle speed of 40 km/h has been tested on ride tests, and 80 km/h has been tested for handling tests. It is found that the results of a higher speed test have a better percentage of reduction in roll motion and acceleration, hence ensuring the stability of the vehicle at high-speed maneuvers while keeping it comfortable. Since higher speed tests are more critical, those results are discussed in this paper.

4.5 Discussion

Overall, all the results do not exceed 5.886 m/s of lateral acceleration meaning that no tests have reached the rollover threshold. Moreover, A.ARB configuration performance is much better than P.ARB which the enviro 500 is using. By observing handling graph in Figure 9-21 although P.ARB has successfully obtained higher performance compared to without ARB configuration, the maximum amplitude of roll angle and roll rate are almost as high with a faster settling time from P.ARB. Some of the results show that P.ARB is not improving the performance rather it is worsening the performances as tested on ISO3888-1 and ISO3888-2. This is because ISO3888-1 involves a very aggressive steering input where P.ARB is having insignificant flexibility to react to the changes. On the other hand, A.ARB can maintain its performance because of the flexibility of the roll stiffness decided by the controller according to situations.

Other than that, the performance of bounce acceleration in the ride test and lateral acceleration in handling test, both the passive and active anti-roll bar failed to give significant improvement in handling tests. Although there is an improvement on bounce acceleration, on the other hand, performance of lateral acceleration is worsened by -4.16% on ISO3888-1 test and -1.28% on ISO3888-2. This is because the main function of the anti-roll bar is to reduce the roll and roll rate (Hamdi et. al., 2024). These will only directly affect vehicle's body roll. The downside is, this will cause the whole vehicle to be stiffer and rigid when A.ARB sensor detects the vehicle's body roll. Hence, causes the vehicle to experience more lateral acceleration. However, the lateral acceleration performance is worsened by only -2.22% through all tests. On the other hand, bounce acceleration can slightly improve by P.ARB due to the extra constant stiffness but as for A.ARB shows better performance is due to the active forces given by the controller.

5.0 CONCLUSION

A full car, 3-axle mathematical model consisting of 20DOF was successfully modeled and simulated within Matlab/Simulink environment. Throughout all results tested, it is proven that the active anti-roll bar was able to have up to an 86.93% improvement of comfort in roll rate on average, reducing roll angle up to 95.07% on average and 32.11% improvement of bounce comfort on average compared to P.ARB used in Enviro 500. Other than that, all handling tests have passed the rollover test by not reaching the rollover threshold in every test. On average, in every handling test, active anti-roll bar is able to reduce roll angle at least up to 98% and roll rate comfort has been improved up to at least 90% and successfully prevents it from reaching more than 96% compared to P.ARB. Unfortunately, it is shown that active anti-roll bar must scarify some of the performance on lateral acceleration to obtain the improvement on roll rate and roll angle in handling test. However, the scarification is very low to negligible with an average of -2.22%. For future improvement, it is recommended to do it with an experimental approach. Experimental data will show better picture of the effectiveness of the proposed controllers, as the simulation in this study only include results with ideal flat plane road inputs. ■

ACKNOWLEDGMENTS

First and foremost, the authors would like to express their sincere gratitude to Mr. Loo Tze Peng, for his invaluable hard work, support, and cooperation throughout this research. The authors also acknowledge the support and collaboration of colleagues at Tunku Abdul Rahman University of Management & Technology. Their heartfelt appreciation goes to the peers and colleagues, whose insightful discussions and suggestions have greatly enriched their work. In particular, they are thankful to Inti International University for their collaborative spirit and technical support.

AUTHORS' CONTRIBUTIONS

Vijayapragas Muniandy	Conceptualisation, study design, and supervision.
Tze Peng Loo	Data collection, methodology, and formal analysis.
Jeyagopi Raman	Writing review, editing, and final manuscript approval.
Sudesh Nair Baskara	Writing review, editing, and final manuscript approval.

REFERENCES

[1] Abu, B.S.A., Samin, P. M., & Azhar, A.A. (2014). Modelling and Validation of Vehicle Ride Comfort Model. *Applied Mechanics and Materials*. 554. 515-519. https://doi.org/10.4028/www.scientific.net/AMM.554.515

[2] Adams, T.A. M. S. (2024). Adams Tire User's Guide, 2024.1. https://nexus.hexagon.com/documentationcenter/csCZ/bundle/Adams_2024.1_Adams_Tire_User_Guide/resource/Adams_2024.1_Adams_Tire_User_Guide.pdf

[3] Ahmed, A. A. (2017). Using of Fuzzy PID Controller to improve Vehicle Stability for Planar Model and Full Vehicle Models. *International Journal of Applied Engineering Research*. 12(5). 671-680. https://www.researchgate.net/publication/316995617_Using_of_fuzzy_pid_controller_to_improve_vehicle_stability_for_planar_model_and_full_vehicle_models

[4] Belrzaeg, M., Almabrouk, A.Q., Khaleel, M., Ahmed, A.A., Ahmed A.A, & Almukhtar, M. (2021). Vehicle dynamics and tire models: An overview. *World Journal of Advanced Research and Reviews*. 12. 331-348. https://doi.org/10.30574/wjarr.2021.12.1.0524

[5] Brian, R. H. M. (2002). *Inertia valve shock absorber*. (United State Patent US 6457730 B1). U.S. Patent and Trademark Office. https://patentimages.storage.googleapis.com/0a/3a/8a/680e59e88bfbc1/US7163222.pdf

[6] Conover, S. G. (2004). *Vehicle Stabilizer Bars with Variable Stiffness Characteristics*. (United State Patent US 6832772 B2). U.S. Patent and Trademark Office. https://yadda.icm.edu.pl/baztech/element/bwmeta1.element.baztech-30b98120-2583-4f64-a3e3-3e461ad41ffe/c/AM74_06_macikowski_EN.pdf

[7] Darus, R. & Yahaya Md. (6-8 March 2009). *Modeling and control of active suspension for Full car model*. 5th International Colloquium on Signal Processing & Its Applications. Kuala Lumpur, Malaysia. https://doi.org/10.1109/CSPA.2009.5069178

[8] Frey, N. W. (2009). Development of rigid ring tire model and comparison among various tire models for ride comfort simulations," *The graduate school of Clemson University*. https://open.clemson.edu/all_theses/615

[9] Gauchia, A., Diaz, V., Boada, M.J.L, Olatunbosun, O.A., & Boada, B.L. (2010). Bus Structure Behavior under Driving Maneuvering and Evaluation of the Effect of an Active Roll System. *International Journal of Vehicle Structures and System, 2*(1), 14-15. https://doi.org/10.4273/ijvss.2.1.03

[10] Gillespie, T. D. (2021). Fundamentals of Vehicle Dynamics. *Fundamentals of Vehicle Dynamics*. Revised Ed. R-506, warren dale, Society of Automotive Engineers, Inc.,125-325. https://doi.org/10.4271/R-506

[11] Hamdi, M. H., Ahmad, F., Che Hasan, M. H., Harun, M. H., & Aparow, V. R. (2024). Model Reference Adaptive Control of an Independent Steer-by-Wire System: A Simulation Using a 14-Degree-of-Freedom Vehicle Model. *International Journal of Automotive and Mechanical Engineering. 21*(4). 11723–11743. https://doi.org/10.15282/ijame.21.4.2024.1.0904

[12] Hans, B.P. (2012). Tire and Vehicle Dynamics. *3rd Ed., Elsevier LTD*. Netherlands. https://doi.org/10.30574/wjarr.2021.12.1.0524

[13] Harnoor Singh, Ekjyot Singh, & Inderjeet, K. (2025). Mechanism Design and Review of Steering System. *TechRxiv*. https://doi.org/10.36227/techrxiv.176592044.49658621/v1

[14] International Organization for Standardization. (2011). *Passenger cars -- Test track for a severe lane-change maneuver -- Part 2: Obstacle avoidance*. ISO 3888-2. https://www.iso.org/standard/57253.html

[15] International Organization for Standardization. (2018). *Passenger cars -- Test track for a severe lane-change maneuver -- Part 1: Double lane-change*. ISO 3888-1. https://licensedcertifiersassociation.com.au/wp-content/uploads/2023/11/Standards-for-Passengers-Cars-1.pdf

[16] Jabatan Kerja Raya (2015). Garis Panduan Pembinaan Bonggol Jalan. *Majlis perbandaran seberang perai, Malaysia*. https://www.mbsp.gov.my/brgonline/garispanduan/kej/bonggol.pdf

[17] Jabatan Kerja Raya. (1985). A Guide on Geometric Design of Roads. *Road Branch Public Works Department.* Malaysia. http://epsmg.jkr.gov.my/images/8/80/5._Bonggol_Jalan_2021.pdf

[18] Joga, D. S., Mochamad, S. & Amrik, S.P.S. (2009). Modeling, simulation and validation of 14 DOF full vehicle model. *The graduate school of Clemson University*. https://doi.org/10.1109/ICICI-BME.2009.5417285

[19] Kuo, Y.-P. & Li, T.H.S. (1999). GA-Based Fuzzy PI/PD Controller for automotive active suspension system. *IEEE Transactions on Industrial Electronics*, 46(6). 1051-1056. https://doi.org/10.1109/41.807984

[20] Manap, A.R.A., Baharom, M., & Maharun, M. (2016). Prediction model of rollover threshold of a high deck bus in quasi static constant radius cornering. *Journal of Scientific Research and Development*. 3(2). 87-91. https://www.ijtsrd.com/archive/10/volume-2/issue-3

[21] Muniandy, V., Samin, P.M., & Jamaluddin, H. (2015). Application of a self-tuning fuzzy PI-PD controller in an active anti-roll bar system for a passenger car. *Vehicle System Dynamics*, 53(11).1641-1666. https://doi.org/10.1080/00423114.2015.1073336?urlappend=%3Futm_source%3Dresearchgate.net%26utm_medium%3Darticle

[22] Noraishikin, Z., Hairi, Z., & Saiful, A.M. (2014). Ride and handling analysis for an active anti-roll bar: case study on composite nonlinear control strategy. *International Journal of Automotive and Mechanical Engineering*, 10(1). 2122-2242. https://doi.org/10.15282/ijame.10.2014.28.0179

[23] Pivonka, P. (May 12-17, 2002). *Comparative analysis of fuzzy PI/PD/PID controller based on classical PID controller approach*. 2002 IEEE World Congress on Computational Intelligence. 2002 IEEE International Conference on Fuzzy Systems. FUZZ-IEEE'02. Proceedings (Cat. No.02CH37291). Honolulu, Hawaii. https://doi.org/10.1109/FUZZ.2002.1005048

[24] Prochowski, L. & Zielonka, K. (2014). Analysis of the Risk of Double-Deck Bus Rollover at the Avoidance of an Obstacle (Analytical Approach and Computer Simulation). *Eksploatacja i Niezawodnosc - Maintenance and Reliability*. 16(4). 507-517. https://www.researchgate.net/publication/292598466_Analysis_of_the_risk_of_double-deck_bus_rollover_at_the_avoidance_of_an_obstacle_analytical_approach_and_computer_simulation

[25] Ross, T. J. (2010). *Fuzzy Logic with Engineering Applications*. University of Mexico, USA: John Wiley & Sons. https://onlinelibrary.wiley.com/doi/book/10.1002/9781119994374

[26] Slade, L.J. (2009). *Development of a new off-road rigid ring model for truck tires using finite element analysis techniques*. [Master Thesis] The Pennsylvania State University. https://etda.libraries.psu.edu/catalog/10075

[27] Solah, M., Ariffin, A., Hafzi, M., & Isa, M. (2013). In-Depth Crash Investigation on Bus Accidents in Malaysia. *Journal of Society for Transportation and Traffic Studies* 3 (1), 22-31, Thailand. https://www.scribd.com/document/620817858/IN-DEPTH-CRASH-INVESTIGATION-ON-BUS-ACCIDENTS-IN-MALAYSIA

[28] Uil, R.T., Besselink, I.J.M., Nijmeijer, H., Schmeitz, A.J.C., & Dommelen, J.A.W. (2007). Tyre models for steady-state vehicle handling analysis. *Eindhoven University of Technology*, Eindhoven. https://api.semanticscholar.org/CorpusID:114085254

[29] Vu, V.-T. (2017). *Enhancing the roll stability of heavy vehicles by using an active anti-roll bar system:* [Doctoral dissertation, Communauté Université Grenoble Alpes]. https://www.researchgate.net/publication/320866850_Enhancing_the_roll_stability_of_heavy_vehicles_by_using_an_active_anti-roll_bar_system

[30] Vu, V.-T., Sename, O., Dugard, L., & Gaspar, P. (2016). Active anti-roll bar control using electronic servo valve hydraulic damper on single unit heavy vehicle. *IFAC-PapersOnLine*, 49(11). 418-425. https://doi.org/10.1016/j.ifacol.2016.08.062

[31] Vu, V.-T., Sename, O., Dugard, L., & Gaspar, P. (2016). H∞ active anti-roll bar control to prevent rollover of heavy vehicles: a robustness analysis. *IFAC-PapersOnLine*, 49(9). 99-104. https://doi.org/10.1016/j.ifacol.2016.07.503

PROFILES

VIJAYAPRAGAS MUNIANDY completed his PHD from University Technology Malaysia in 2016, majoring in Automotive Engineering. 9 years of research experience and teaching undergraduate and postgraduate students at Inti International University. He obtained professional engineer status in 2019.
Email address: vijay.muniandy@newinti.edu.my

TZE PENG LOO completed his Bachelor's Degree in Mechanical Engineering in Tunku Abdul Rahman University of Management and Technology (2019). Currently working as Technical Assistant Manager at SMC Corporation, Singapore.

JEYAGOPI RAMAN is currently a Lecturer in Engineering Department at the INTI International University, Nilai, Malaysia since 2002; and he has been a senior lecturer since 2012. He received his BEng degree in Electronic and Electrical Engineering from Robert Gordan University, UK in 1998; MSc degree in Mechatronic from De Montfort University, UK in 1999 and Ph.D. degree in Electrical Power Engineering from Universiti Tenaga Nasional, Malaysia in 2016. His research interests include in the field of power system, power quality, power electronics, motor controller, renewable energy, industrial application, robotics, artificial intelligence, and intelligent control.
Email address: jeyag.raman@newinti.edu.my

SUDESH NAIR BASKARA is the Head of Programme (HOP) for Civil Engineering in Inti International University, Nilai. He has completed his PhD in Highway and Transportation in year 2022. He has been involved in civil engineering for 14 years, spanning both academia and industry. Besides teaching Highway and Transportation, he also teaches land surveying. He is involve in research of road accident analysis and has published a number of research papers.
Email address: sudesh.baskara@newinti.edu.my